

A significance test for mixed-integer models with application to GNSS

Teunissen, Peter J.G.

10.1007/s10291-025-01952-3

Publication date

Document Version Final published version

Published in **GPS Solutions**

Citation (APA)

Teunissen, P. J. G. (2025). A significance test for mixed-integer models with application to GNSS. *GPS Solutions*, *29*(4), Article 200. https://doi.org/10.1007/s10291-025-01952-3

Important note

To cite this publication, please use the final published version (if applicable). Please check the document version above.

Copyright
Other than for strictly personal use, it is not permitted to download, forward or distribute the text or part of it, without the consent of the author(s) and/or copyright holder(s), unless the work is under an open content license such as Creative Commons.

Takedown policy

Please contact us and provide details if you believe this document breaches copyrights. We will remove access to the work immediately and investigate your claim.

RESEARCH



A significance test for mixed-integer models with application to GNSS

Peter J. G. Teunissen 1,2,3

Received: 4 June 2025 / Accepted: 24 August 2025 © The Author(s) 2025

Abstract

GNSS model validation constitutes an essential part of any GNSS data processing scheme. With the inclusion of the very precise, but integer ambiguous carrier-phase data, the GNSS models become of the mixed-integer type. Although inference theory of mixed-integer models is well developed for parameter estimation, this is not yet the case for the validity testing of such models. It is the goal of this contribution to help close this gap by introducing the ambiguity-resolved parameter significance test. It differs from existing significance tests in that it takes the unknown integerness of the ambiguities rigorously into account. Our analysis shows that the proposed test can significantly outperform currently used tests.

Keywords GNSS · Mixed integer models · Significance testing · Ambiguity-resolved significance test · Power functions · Integer ambiguity resolution

Introduction

GNSS model validation constitutes an essential part of any GNSS data processing scheme (Leick et al. 2015; Teunissen et al. 2017). Statistical tests are then employed to test for the occurrence of model misspecifications, such as pseudorange (code) outliers, carrier-phase slips, neglected atmospheric delays, or lack of parameter stability, such as in time-series for displacement, deformation or landslide studies (Perfetti 2006; Khanafseh et al. 2012; Teunissen and Bakker 2013; Biagi et al. 2016; Yu et al. 2023; Zeng et al. 2023; Huang et al. 2023). To achieve the best possible precision in GNSS parameter estimation, carrier-phase measurements are used, as they are two orders more precise than their pseudorange counterparts. Strang and Borre (1997), Hofmann-Wellenhof et al. (2008), Morton et al. (2020). However, since the carrier-phase observables are integer ambiguous, their GNSS models consist of both real-valued and integervalued parameters, and are therefore of the mixed-integer

type. Although the theory of mixed-integer inference is well developed for GNSS parameter estimation (Teunissen 2010; Teunissen et al. 2017; Morton et al. 2020), such is not yet the case for the validity testing of mixed-integer GNSS models. It is the goal of this contribution to contribute to this field by introducing the ambiguity-resolved *significance* test. This test complements the ambiguity-resolved *detector* test that was introduced and studied in Teunissen (2024), Yin et al. (2024), Yin et al. (2025).

This contribution is organized as follows. In Section "Current significance testing", we formulate our null- and alternative hypothesis for the general mixed-integer model and provide a brief overview of its current significance testing. We hereby emphasize in particular the tremendous difference in testing power that exists between the ambiguity-float (AF) and ambiguity-known (AK) significance tests. It is this large difference in power that has motivated us to develop a new significance test for the mixed-integer model. It differs from existing tests in that it takes the unknown integerness of the ambiguities rigorously into account.

In Section "AR-bias estimator and distribution" we determine the integer ambiguity resolved estimator of the to-be-tested model bias, together with its probability distribution. To gain insight into its characteristics, we show how the shape of its multimodal probability density function (PDF) is driven by the interplay between the probability mass function (PMF) of the integer estimated ambiguities and the PDF of the ambiguity-constrained bias-estimator.

Published online: 27 September 2025



Peter J. G. Teunissen p.j.g.teunissen@tudelft.nl

Department of Geoscience and Remote Sensing, Delft University of Technology, Delft, The Netherlands

Department of Infrastructure Engineering, University of Melbourne, Melbourne, Australia

³ GNSS Research Centre, Curtin University, Perth, Australia

This analysis is further made GNSS-specific in Section "Single-epoch GNSS model PDF $f_{\underline{c}}(x)$ ", where we consider a general single-epoch GNSS mixed-integer model.

In Section "The AR significance test", we introduce our ambiguity-resolved significance (ARs) test. To accomodate the multimodality of the test-statistic's PDF, the PDF's highest-density level sets are used, instead of the classical 'p-value' approach, to determine the geometry of the acceptance and rejection regions. We show how the test sits in between the AF- and AK-tests and how it can benefit from the integerness of the ambiguities to significantly outperform the AF-test.

In Section "The AR normed significance test" we demonstrate the importance of properly accounting for the uncertainty of the integer ambiguity estimators. We show the errors-in-testing one makes when this uncertainty is neglected, as is done when using the AK-test. We also show, when this uncertainty is properly taken into account, that the corresponding test, referred to as AR-normed (ARn) test, becomes a good and easy-to-compute, approximation to the ARs-test in case multimodality is absent. To avoid multimodality and allow for a good use of this test, we introduce the concept of partial-ambiguity-resolved significance testing. It is shown how this *partial* ARs-test improves the AF-test and also how it can be combined with the full ARs-test so as to further improve the testing performance. Section "Summary and conclusions" contains the summary and conclusions, and Section "Appendix" the appendix.

The following notation is used throughout: We denote a random variable/vector by means of an underscore; thus xis a random variable/vector, while x is not. E(.) and D(.)denote the expectation and dispersion operators, respectively, and $f_x(x)$ the probability density function (PDF) of x. A variance-covariance matrix, we usually refer to as a vc-matrix or simply as a variance matrix. \mathbb{Z}^n denotes the *n*-dimensional space of integer numbers and \mathbb{R}^p the *p*-dimensional space of real numbers. The range space of matrix M is denoted as $\mathcal{R}(M)$. Matrix $M^+ = (M^T Q_{yy}^{-1} M)^{-1} M^T Q_{yy}^{-1}$ denotes the BLUE-inverse of the full column rank matrix M, and $P_M = MM^+$ and $P_M^{\perp} = I_m - P_M$ are the orthogonal projectors that project on the range space of M and its orthogonal complement, respectively. The squared weighted norm is denoted as $||.||_R^2 = (.)^T R^{-1}(.)$. $\mathcal{N}_m(\mu, Q)$ denotes the *m*-variate normal distribution with mean μ and variance matrix Q, and $\chi^2(q,\lambda)$ denotes the noncentral Chi-square distribution with q degrees of freedom and noncentrality parameter λ . The determinant of a matrix Q is denoted as |O|. P[E] denotes the probability of event E and A^c denotes the set complementary to A.



In this section we describe our hypotheses, as well as provide a brief comparative review of the ambiguity-float (AF) and ambiguity-known (AK) tests. They form the limiting versions of the integer ambiguity resolved significance tests that we will introduce in the sections following.

The null- and alternative hypothesis

With our vector of observables distributed as $\underline{y} \sim \mathcal{N}_m$ $(E(y), Q_{yy})$, and its mean parametrized as

$$E(y) = Aa + Bb + Cc, \quad a \in \mathbb{Z}^n, \quad b \in \mathbb{R}^p, \quad c \in \mathbb{R}^q$$
 (1)

we aim to test the hypotheses

$$\mathcal{H}_0: c = 0 \quad \text{versus} \quad \mathcal{H}_a: c \neq 0$$
 (2)

whereby the given matrix $[A, B, C] \in \mathbb{R}^{m \times (n+p+q)}$ is assumed to be of full column-rank. A prime example of model (1) is given by the linearized model of GNSS observation equations, with $y \in \mathbb{R}^m$ containing the carrierphase and pseudorange observables, $a \in \mathbb{Z}^n$ the unknown integer carrier-phase ambiguities, and $b \in \mathbb{R}^p$ and $c \in \mathbb{R}^q$, the unknown real-valued parameters, such as e.g. position coordinates, atmosphere parameters, receiver and satellite clock parameters, and instrumental biases (Strang and Borre 1997; Leick et al. 2015; Teunissen et al. 2017). With (2) the aim is then to test for the significance of the entries in the q-vector c, i.e. to answer the question whether its entries can be considered small enough to be neglected. Through a proper choice of c one can then test for the presence of, for instance, tropospheric delays, ionospheric delays, pseudorange outliers, carrier phase cycle slips, or any of the other parameters in the model.

We remark that a more general formulation of (1) and (2) would be

$$E(y) = Aa + Hx, \quad a \in \mathbb{Z}^n, \quad x \in \mathbb{R}^{p+q}$$
(3)

with hypotheses

$$\mathcal{H}_0: F^T x = 0 \quad \text{versus} \quad \mathcal{H}_a: F^T x \neq 0$$
 (4)

whereby $F \in \mathbb{R}^{(p+q) \times q}$ is of rank q. In this case it are the q functions F^Tx that are to be tested for significance. By taking H = [B,C] and $F^T = [0,I_q]$ we obtain (1) and (2) again, thus showing that they are indeed a special case. Nevertheless, in this contribution we will work with formulation (1) and (2) as it does not pose any restriction on the generality of our theory development. The general



GPS Solutions (2025) 29:200 Page 3 of 16 200

formulation of (3) and (4) can namely always be brought into the form of (1) and (2). To see this, we reparametrize x as $x = F^{\perp}b + F^{+}c$, in which F^{\perp} is a basis matrix of the null space of F^{T} and $F^{+} = F(F^{T}F)^{-1}$. Then $F^{T}x = c$ and $[HF^{\perp}, HF^{+}] = [B, C]$.

We finally remark that an even more general formulation than (4) would be one in which the integer parameter vector $a \in \mathbb{Z}^n$ would also be taking part in the null-hypothesis \mathcal{H}_0 . Such mixed form of significance testing is however outside the scope of the present work.

The AF and AK significance test

An important complication of formulation (1) is the presence of the integer ambiguity vector $a \in \mathbb{Z}^n$. No proper significance testing is currently in place that incorporate this integerness. What currently is done is to either disregard the integerness of the ambiguities and thus work as if $a \in \mathbb{R}^n$, or alternatively, with reference to the output of ambiguity resolution, to treat the ambiguities as if they are known. We will refer to the significance tests of these two cases as the ambiguity-float (AF) significance test and the ambiguity-known (AK) significance test.

If we denote the Best Linear Unbiased Estimator (BLUE) of c as \hat{c} , when a is treated as an unknown real-valued vector, and as $\hat{c}(a)$, when a is assumed known, the two corresponding significance tests read

Reject
$$\mathcal{H}_0$$
 if
$$\begin{cases} AF : ||\hat{c}||_{Q_{\hat{c}\hat{c}}}^2 > k_{\alpha} \\ AK : ||\hat{c}(a)||_{Q_{\hat{c}(a)\hat{c}(a)}}^2 > k_{\alpha} \end{cases}$$
 (5)

and accept \mathcal{H}_0 otherwise. To be able to evaluate and compare these two tests, we need their distributions. Since $\underline{\hat{c}} \sim \mathcal{N}_q(c,Q_{\hat{c}\hat{c}})$ and $\underline{\hat{c}}(a) \sim \mathcal{N}_q(c,Q_{\hat{c}(a)\hat{c}(a)})$, we have

$$||\underline{\hat{c}}||_{Q_{\hat{c}\hat{c}}}^2 \sim \chi^2(q, \lambda_{\hat{c}})$$

$$||\underline{\hat{c}}(a)||_{Q_{\hat{c}(a)\hat{c}(a)}}^2 \sim \chi^2(q, \lambda_{\hat{c}(a)})$$
(6)

with noncentrality parameters

$$\lambda_{\hat{c}} = ||c||_{Q_{\hat{c}(a)}}^2 \quad \text{and} \quad \lambda_{\hat{c}(a)} = ||c||_{Q_{\hat{c}(a)\hat{c}(a)}}^2$$
 (7)

As the two test-statistics have under \mathcal{H}_0 the same central Chi-square distribution with q degrees of freedom, they can indeed work with the same critical value $k_{\alpha}=\chi_{\alpha}^2(q,0)$, cf. (5), thus providing their same probability of false alarm as $\mathrm{P}[||\underline{\hat{c}}||_{Q_{\hat{c}(a)\hat{c}(a)}}^2>k_{\alpha}|\mathcal{H}_0]=\mathrm{P}[||\underline{\hat{c}}(a)||_{Q_{\hat{c}(a)\hat{c}(a)}}^2>k_{\alpha}|\mathcal{H}_0]=\alpha$.

The following Lemma provides the necessary information for comparing the power performance of the two tests.

Lemma 1 (Bias precision and noncentrality) The vc-matrices of the BLUEs $\underline{\hat{c}}$ and $\underline{\hat{c}}(a)$, and the relation between the noncentrality parameters of (7), are given as

$$Q_{\hat{c}\hat{c}} = [\bar{C}^T Q_{yy}^{-1} \bar{C}]^{-1}, \quad \text{with} \quad \bar{C} = P_{[A,B]}^{\perp} C$$

$$Q_{\hat{c}(a)\hat{c}(a)} = [\bar{C}^T Q_{yy}^{-1} \bar{C}]^{-1}, \quad \text{with} \quad \bar{C} = P_B^{\perp} C$$

$$\lambda_{\hat{c}(a)} = \lambda_{\hat{c}} + ||P_{\bar{A}} C c||_{Q_{yy}}^2, \quad \text{with} \quad \bar{A} = P_B^{\perp} A$$
(8)

Proof see Appendix.

Since the integral $\int_{k_{\alpha}}^{\infty} f_{\chi^2(q,\lambda)}(x) dx$ is monotone increasing in λ , and $\lambda_{\hat{c}(a)} \geq \lambda_{\hat{c}}$, it follows for their power that

$$\mathbf{P}[||\hat{\underline{c}}(a)||^2_{Q_{\hat{c}\hat{c}}} > k_{\alpha}|\mathcal{H}_a] \ge \mathbf{P}[||\hat{\underline{c}}||^2_{Q_{\hat{c}(a)\hat{c}(a)}} > k_{\alpha}|\mathcal{H}_a]$$

thus showing that the AF-test is never more powerful than the AK-test. For the noncentrality parameters we have

$$\lambda_{\hat{c}} = 0 \quad \text{if} \quad \mathcal{R}(C) \subset \mathcal{R}([A, B])$$

$$\lambda_{\hat{c}(a)} = 0 \quad \text{if} \quad \mathcal{R}(C) \subset \mathcal{R}(B)$$

$$\lambda_{\hat{c}} = \lambda_{\hat{c}(a)} \quad \text{if} \quad \mathcal{R}(C) \subset \mathcal{R}(P_B^{\perp} A)^{\perp}$$

$$(9)$$

The first relation shows that significance testing of c is impossible if the column vectors of C lie in the range space of [A,B], while the second relation shows that this remains impossible, even when a is known, if the columns of C reside in the range space of B. The third relation stipulates that the two noncentrality parameters are equal if the column vectors of C lie in the orthogonal complement of the range space of $\bar{A} = P_B^{\perp} A$, i.e. if $C^T Q_{yy}^{-1} P_B^{\perp} A = 0$. In this case, \hat{a} , being the BLUE of a, is uncorrelated with \hat{c} , implying that knowing a does not affect the estimator of c, i.e. $\hat{c}(a) = \hat{c}$.

In case of GNSS, the AK-test is driven by the very-precise carrier-phase data. The difference between the AK-test and AF-test can then be quite dramatic, in particular if the AF-test is driven by the relatively poor precision of the pseudorange data. Figure 1 shows such an example, with c being the vertical tropospheric delay for a single-epoch, dual-frequency, short-baseline GPS model.

Strictly speaking, one can of course not apply the above AK-test in case of GNSS. Although the carrier-phase ambiguities are known to be integer, they are still unknown. When the AK-test is currently used in practice, the typical approach is to replace a by its integer estimate \check{a} , thereby treating it as if it is the known ambiguity value. By replacing a in (5) by \check{a} , the test becomes then

Reject
$$\mathcal{H}_0$$
 if $||\hat{c}(\check{a})||^2_{Q_{\hat{c}(a)\hat{c}(a)}} > k_{\alpha} = \chi^2_{\alpha}(q,0)$ (10)



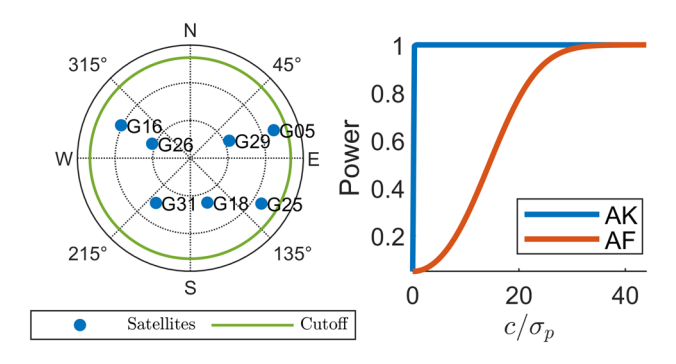


Fig. 1 Tropospheric AK and AF power function curves, computed using their noncentral Chi-square cumulative distribution function (CDF). Left: single-epoch GPS skyplot; Right: single-epoch, L1/L2 geometry-based GPS, ambiguity-float (AF) and ambiguity-known (AK) power function curves for $\alpha=0.05$ tropospheric zenith delay testing, with c/σ_p being the ratio of the vertical tropospheric delay and pseudorange standard deviation

But due to the randomness of $\underline{\check{a}}$, this is *not* a correct way of performing the test. The random variable $||\underline{\hat{c}}(\underline{\check{a}})||^2_{Q_{\hat{c}(a)\hat{c}(a)}}$ will namely not have the Chi-square distribution that $||\underline{\hat{c}}(a)||^2_{Q_{\hat{c}(a)\hat{c}(a)}}$ of (6) has. This implies that its level- α critical value can not be computed as $k_{\alpha} = \chi^2_{\alpha}(q,0)$ and that its detection probabilities will not be those of the AK-test.

AR-bias estimator and distribution

To develop a proper test, we first need to take the randomness of the estimated integer ambiguities in the expression of the ambiguity-resolved bias-estimator $\underline{\check{c}} = \underline{\hat{c}}(\underline{\check{a}})$ into account. This is achieved by determining the PDF of \check{c} .

Theorem 1 (PDF of AR-bias estimator) The PDF of $\underline{\check{c}} = \hat{c}(\check{a})$ is given as

$$f_{\underline{\check{c}}}(x) = \sum_{z \in \mathbb{Z}^n} f_{\underline{\hat{c}}(z)}(x) P[\underline{\check{a}} = z]$$
(11)

with $f_{\underline{\hat{c}}(z)}(x)$ the PDF of $\underline{\hat{c}}(z) \stackrel{\mathcal{H}_a}{\sim} \mathcal{N}_q(c + \bar{C}^+ A(a - z),$ $Q_{\hat{c}(a)\hat{c}(a)} = (\bar{C}^T Q_{yy}^{-1} \bar{C})^{-1}), \ \bar{C}^+ A = -Q_{\hat{c}\hat{a}} Q_{\hat{a}\hat{a}}^{-1},$ $P[\underline{\check{a}} = z] = \int_{S_z} f_{\hat{a}}(\alpha) d\alpha$ the PMF of $\underline{\check{a}}, f_{\hat{a}}(\alpha)$ the PDF of $\underline{\hat{a}} \stackrel{\mathcal{H}_a}{\sim} \mathcal{N}_n(a, Q_{\hat{a}\hat{a}} = (\bar{\bar{A}}^T Q_{yy}^{-1} \bar{\bar{A}})^{-1}), \ \bar{\bar{A}} = P_{[B,C]}^{\perp} A, \ and$ $S_z \subset \mathbb{R}^n$ the pull-in region of the integer ambiguity estimator \check{a} .

It is not difficult to verify that the PDF of $\underline{\check{c}}$ is symmetric about c, $f_{\underline{\check{c}}}(c-x) = f_{\underline{\check{c}}}(c+x) \ \forall x \in \mathbb{R}^n$, at which point it reaches its maximum, $f_{\underline{\check{c}}}(c) \geq f_{\underline{\check{c}}}(x) \ \forall x \in \mathbb{R}^n$. Its

symmetry about c confirms that the AR-bias estimator $\underline{\check{c}}$ is an *unbiased* estimator of c. We also remark that this property, as well as expression (11), hold true for any unbiased integer estimator $\underline{\check{a}}$ one chooses from the class of admissible integer estimators (Teunissen 2003). Popular choices are integer rounding (IR) or integer bootstrapping (IB) (Teunissen 1998), both of which are very simple to execute, or the more involved integer least-squares (ILS) which was shown by Teunissen (1999) to have the largest possible probability of correct integer estimation. Even combinations of these integer estimators are possible (Teunissen et al. 2021).

Expression (11) shows that the PDF $f_{\underline{\check{c}}}(x)$ is an infinite sum of $\bar{C}^+A(a-z)$ -shifted and $P[\underline{\check{a}}=z]$ -downweighted, but equally $(\bar{C}^TQ_{yy}^{-1}\bar{C})^{-1}$ -peaked, normal distributions. The PDF of $\underline{\check{c}}$ will therefore be multimodal in general, with its shape governed by the following three drivers:

- 1. $Q_{\hat{c}(a)\hat{c}(a)}$: peakedness of PDF $f_{\hat{c}(z)}(x)$
- 2. $Q_{\hat{a}\hat{a}}$: peakedness of PMF $P[\underline{\check{a}}=z]$
- 3. $Q_{\hat{c}\hat{a}}Q_{\hat{a}\hat{a}}^{-1}z$: shift size of $f_{\hat{c}(z)}(x)$

To get some further insight into the characteristics of the multimodal PDF and the different shapes that it can take, we consider the scalar case as illustration. In the scalar case, the integer estimator $\underline{\check{a}}$ simply boils down to rounding $\underline{\hat{a}}$ to the nearest integer, denoted as $\lfloor \underline{\hat{a}} \rfloor$. For n=q=1, $\underline{\hat{a}} \sim \mathcal{N}(a=0,\sigma_{\hat{a}}^2)$ and $\gamma=\sigma_{\hat{c}\hat{a}}\sigma_{\hat{a}}^{-2}$, expression (11) simplifies then to

$$f_{\underline{\check{c}}}(x) = \sum_{z \in \mathbb{Z}} \mathcal{N}(\gamma z, \sigma_{\hat{c}(a)}^2) P[\lfloor \underline{\hat{a}} \rceil = z]$$
(12)

with ambiguity PMF

$$P[\lfloor \underline{\hat{a}} \rceil = z] = \Phi\left(\frac{1 - 2z}{2\sigma_{\hat{a}}}\right) + \Phi\left(\frac{1 + 2z}{2\sigma_{\hat{a}}}\right) - 1$$

in which $\Phi(x)=\int_{-\infty}^x \frac{1}{\sqrt{2\pi}}e^{-\frac{1}{2}v^2}dv$. The three parameters that drive the characteristics of the PDF (12) are therefore,

- 1. $\sigma_{\hat{c}(a)}$: peakedness of PDF $\mathcal{N}(\gamma z, \sigma^2_{\hat{c}(a)})$.
- 2. $\sigma_{\hat{a}}$: peakedness of PMF $P[\lfloor \hat{\underline{a}} \rceil = z]$.
- 3. γ : shift size of $\mathcal{N}(\gamma z, \sigma_{\hat{c}(a)}^2)$.

To illustrate the different shapes the PDF $f_{\underline{c}}(x)$ can have, we take two values (small and large) for the three parameters $\sigma_{\hat{c}(a)}$, $\sigma_{\hat{a}}$ and γ , thus resulting in $2^3=8$ different PDF versions, all of which are shown in Fig. 2. The PDFs in the top row differ from those in the bottom row only through $\sigma_{\hat{c}(a)}$. This explains the spikey behaviour seen in the top row $(\sigma_{\hat{c}(a)}$ small) versus the smoother behaviour in the bottom row $(\sigma_{\hat{c}(a)}$ large). The influence of the peakedness of the



GPS Solutions (2025) 29:200 Page 5 of 16 200

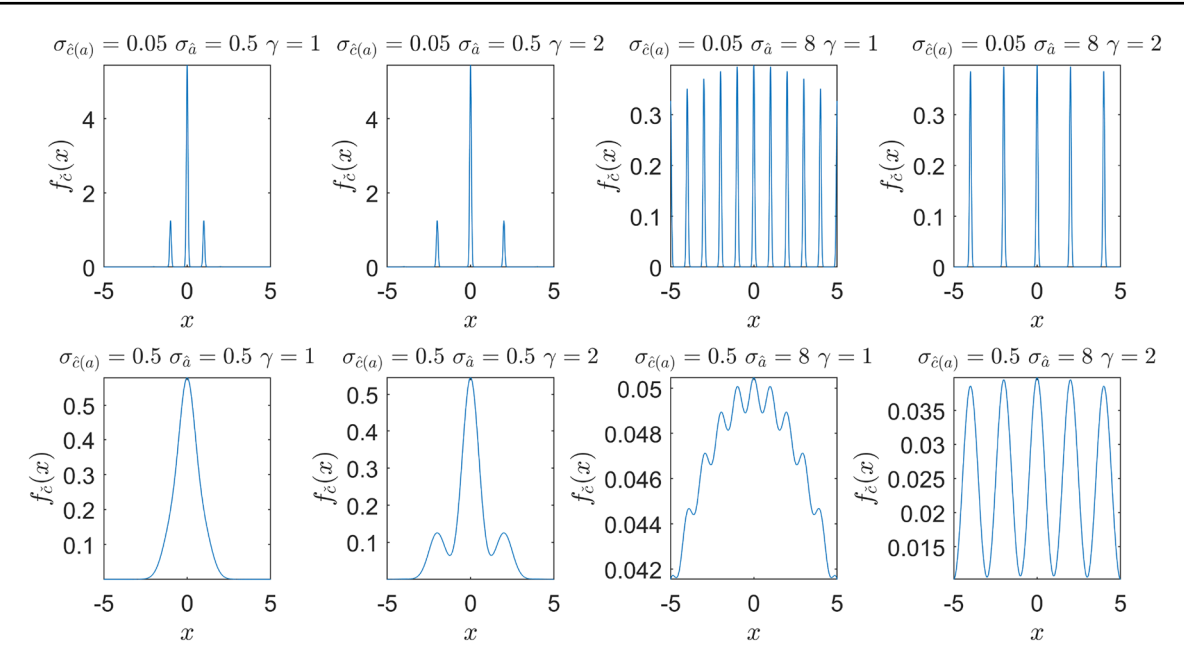


Fig. 2 Shapes of the PDF $f_{\underline{c}}(x) = \sum_{z \in \mathbb{Z}} \mathcal{N}(\gamma z, \sigma_{\hat{c}}^2) P[\check{a} = z]$ for different values of $\sigma_{\hat{c}(a)}$ (compare top row with bottom row), $\sigma_{\hat{a}}$ (compare first two columns with last two columns), $\gamma = \sigma_{\hat{c}\hat{a}}\sigma_{\hat{a}}^{-2}$ (compare first and third column with second and last column)

ambiguity PMF can be seen when one compares the PDFs of the first two columns ($\sigma_{\hat{a}}$ small) with those in the last two colums ($\sigma_{\hat{a}}$ large). The multimodality of the PDF increases, the less peaked the ambiguity PMF is, i.e. the larger $\sigma_{\hat{a}}$ is. Finally, the effect of the shifts γz can be seen when comparing the PDFs in the first and third column with those in the second and fourth column. It shows for instance, that a multi-peaked ambiguity PMF might still produce a unimodal PDF if the shifts γz are small enough and the standard deviation $\sigma_{\hat{c}(a)}$ large enough.

Single-epoch GNSS model PDF $f_{\check{c}}(x)$

To characterize the PDF $f_{\underline{c}}(x)$ for GNSS, we show in this section how the above mentioned three drivers work out for an f-frequency, m double-differenced (DD) pseudorange and carrier-phase geometry-based model, see e.g. Teunissen et al. (2017). We consider the most challenging case, being a single-epoch model under a general alternative hypothesis,

$$\mathcal{H}_a: \mathbf{E} \left[\begin{array}{c} \underline{p} \\ \underline{\phi} \end{array} \right] = \left[\begin{array}{cc} 0 & G & C_p \\ L & G & C_{\phi} \end{array} \right] \left[\begin{array}{c} a \\ b \\ c \end{array} \right], \tag{13}$$

with $\mathrm{D}(\underline{p})=Q_{pp}=\sigma_p^2Q,\, \mathrm{D}(\underline{\phi})=Q_{\phi\phi}=\sigma_\phi^2Q,\,\underline{p}$ uncorrelated with $\underline{\phi}$, and both normally distributed. In (13), the pseudorange and carrier-phase data are collected in $\underline{p},\underline{\phi}\in\mathbb{R}^{fm}$, the fm integer DD ambiguities in $a\in\mathbb{Z}^{fm}$, the real-valued GNSS parameters, like baseline components and possibly

atmospheric delays, in $b \in \mathbb{R}^p$, and the hypothesized q model biases in $c \in \mathbb{R}^q$. The design matrices in (13) are: $L = \Lambda \otimes I_m \in \mathbb{R}^{fm \times fm}$, with $\Lambda = \operatorname{diag}(\lambda_1, \dots, \lambda_f)$ and λ_i the wavelength of the ith frequency; $G = e_f \otimes \mathcal{G} \in \mathbb{R}^{fm \times p}$, with e_f the f-vector of ones and $\mathcal{G} \in \mathbb{R}^{m \times p}$ the DD receiver-satellite geometry matrix; and $C_p, C_\phi \in \mathbb{R}^{fm \times q}$ the signature matrices that link the hypothesized model bias with the observables.

We assume the bias vector $c \in \mathbb{R}^q$ to be fully estimable under \mathcal{H}_a and therefore the design matrix of (13) to be of full column rank. This implies, as also the design matrix under \mathcal{H}_0 , i.e. when c=0, is assumed to be of full rank, that linear combinations of the q columns of $[C_p^T, C_\phi^T]^T$ cannot lie in the range space of the first n+p columns of the design matrix of (13). Note that this also implies that C_p cannot be zero. Would $C_p=0$, then the invertibility of L implies that the last q columns of the design matrix become linear dependent on the first n, as a result of which the design matrix of (13) becomes rank defect.

The following theorem provides the drivers that characterize the PDF $f_{\underline{c}}(x)$ for the GNSS model (13).

Theorem 2 (GNSS PDF $f_{\underline{\hat{c}}}(x)$ characterized) For the single-epoch GNSS model (13), the vc-matrices of $\underline{\hat{c}}$ and $\underline{\hat{c}}(a)$, the integer driven shift of the bias $\Delta(z) = E(\underline{\hat{c}}(z) - c)$, and the vc-matrices of $\underline{\hat{c}}(c)$ and $\underline{\hat{c}}(c)$, are given as



$$Q_{\hat{c}\hat{c}} = [\bar{C}_{p}^{T} Q_{pp}^{-1} \bar{C}_{p}]^{-1}$$

$$Q_{\hat{c}(a)\hat{c}(a)} = [Q_{\hat{c}\hat{c}}^{-1} + \bar{C}_{\phi}^{T} Q_{\phi\phi}^{-1} \bar{C}_{\phi} + \frac{\epsilon}{1+\epsilon} D^{T} Q_{\phi\phi}^{-1} D]^{-1}$$

$$\Delta(z) = Q_{\hat{c}(a)\hat{c}(a)} (\bar{C}_{\phi} + \frac{\epsilon}{1+\epsilon} D)^{T} Q_{\phi\phi}^{-1} L(a-z)$$
(14)

and

$$Q_{\hat{a}(c)\hat{a}(c)} = L^{-1} \left(\epsilon Q_{pp} + P_G Q_{pp} \right) L^{-T}$$

$$Q_{\hat{a}\hat{a}} = Q_{\hat{a}(c)\hat{a}(c)} + E Q_{\hat{c}\hat{c}} E^T$$
(15)

with projectors $P_G = G[G^TQ^{-1}G]^{-1}G^TQ^{-1}$ and $P_G^{\perp} = I_{fm} - P_G$, the projected C-matrices $\bar{C}_p = P_G^{\perp}C_p$ and $\bar{C}_\phi = P_G^{\perp}C_\phi$, the phase-code variance-ratio $\epsilon = \sigma_\phi^2/\sigma_p^2$, and $D = P_G(C_\phi - C_p)$, $E = L^{-1}[\bar{C}_\phi + D]$.

Proof see Appendix.

Note that both D and E do not change with σ_{ϕ}^2 and σ_p^2 and that $Q_{\hat{a}(c)\hat{a}(c)}$ is the ambiguity-variance matrix under \mathcal{H}_0 . Furthermore, we remark that the above given matrices \bar{C}_p and \bar{C}_ϕ should not be confused with the earlier defined $\bar{C} = P_B^\perp C$. With the results of the above theorem we are now in a position to provide a qualitative discussion on the driving characteristics of the multimodal PDF of $\underline{\check{c}} = \hat{c}(\underline{\check{a}})$. We first consider the PDF peakedness of $f_{\hat{c}(z)}(x)$, then the PMF peakedness of $P[\check{a} = z]$ as it is driven by the vc-matrix of \hat{a} , and finally the integer-driven bias of $f_{\hat{c}(z)}(x)$.

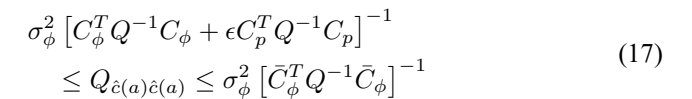
The peakedness of $f_{\hat{c}(z)}(x)$

As the peakedness of this PDF is completely determined by the vc-matrix $Q_{\hat{c}(a)\hat{c}(a)}$, we consider the second equation of (14). To understand when and how the code-precision or phase-precision dominates the precision of $\hat{\underline{c}}(a)$, we need to consider the rank of the $fm \times (p+q)$ matrix $[G, C_{\phi}]$. Its rank is bounded as

$$p \le \operatorname{rank}(G, C_{\phi}) \le p + q \tag{16}$$

The upperbound is clear. The lowerbound follows from the fact that $\mathrm{rank}(G)=p$, which follows from our earlier assumption that the design matrix under \mathcal{H}_0 , i.e. when c=0, is of full column rank. We now consider the two extreme cases: $\mathrm{rank}(G,C_\phi)=p$ and $\mathrm{rank}(G,C_\phi)=p+q$. We start with the upperbound.

Case $\operatorname{rank}(G, C_{\phi}) = p + q$: As matrix $[G, C_{\phi}]$ is of full column rank, the phase data are sufficient to estimate the bias vector c when the ambiguities are known. One can therefore expect the precision of $\underline{\hat{c}}(a)$ to be dominated by the high-precision of the phase data. And indeed, the following lower- and upperbound can then be obtained from (14),



The lowerbound is the variance matrix when also the baseline b would be assumed known, while the upperbound is the phase-only variance matrix. As both the lower- and upperbound are dominated by the very small phase-variance σ_{ϕ}^2 , the PDF $f_{\hat{\underline{c}}(z)}(x)$ can be expected to be peaked in this case.

Case $\operatorname{rank}(G,C_\phi)=p$: Note, as G is of full column rank p, that this case is equivalent to stating that all column vectors of C_ϕ lie in the range space of G, i.e. that $\bar{C}_\phi=P_G^\perp C_\phi=0$. Hence, for the ambiguity-known situation, the inclusion of code data is then needed, as phase data alone will now not be sufficient for estimating the bias vector c. The following lower- and upperbound can then be obtained from (14),

$$\sigma_p^2[(C_p - C_\phi)^T Q^{-1} (C_p - C_\phi)]^{-1}$$

$$\leq Q_{\hat{c}(a)\hat{c}(a)} \leq \sigma_p^2 [\bar{C}_p^T Q^{-1} \bar{C}_p]^{-1}$$
(18)

The upperbound is the code-only variance matrix, while the lowerbound can be understood as follows. With the range space of C_{ϕ} being a subset of $\mathcal{R}(G)$, a matrix X exists such that $C_{\phi} = GX$, thus allowing us to reparametize the ambiguity-known model as

$$E\begin{bmatrix} \underline{p} \\ \underline{\phi} - La \end{bmatrix} = \begin{bmatrix} G & C_p - C_\phi \\ G & 0 \end{bmatrix} \begin{bmatrix} b + Xc \\ c \end{bmatrix}$$
 (19)

The lowerbound of (18) is then the code-only variance matrix of the estimated bias vector, when next to the ambiguities, also the lumped parameter vector b + Xc would be assumed known.

As the bounds of (18) are dominated by the relatively poor precision of the code data, the conclusion is that one cannot expect the PDF $f_{\underline{\hat{c}}(z)}(x)$ to be very peaked when $\bar{C}_{\phi}=0$. As this case includes $C_{\phi}=0$, i.e. the situation when the bias vector is only linked to the code data, a similar conclusion is reached for code or pseudorange outliers.

Also note, when next to $\bar{C}_{\phi}=0$ also $D=P_G$ $(C_{\phi}-C_p)=0$, then $Q_{\hat{c}(a)\hat{c}(a)}=Q_{\hat{c}\hat{c}}$, cf. (14). In this case, integer ambiguity resolution, even when successful, will have no impact at all on the estimator of c. Two examples of such are (i) when Cc models a tropospheric delay for which the vector of mapping functions lies in the range space of G, and (ii) when Cc models a code-bias for which its signature matrix C_p lies in the orthogonal complement of the range space of G.

With respect to Fig. 2 we can now conclude, as far as the peakedness of $f_{\hat{c}(z)}(x)$ is concerned, that the PDF



GPS Solutions (2025) 29:200 Page 7 of 16 200

characteristics of its top-row correspond to the case $\operatorname{rank}(G,C_\phi)=p+q$, while those of the bottom-row correspond to the case $\operatorname{rank}(G,C_\phi)=p$. For the intermediate cases $p<\operatorname{rank}(G,C_\phi)< p+q$, linear combinations of some of the column vectors of C_ϕ will lie in the range space of G, while others will not. In that case the PDF $f_{\underline{\hat{c}}(z)}(x)$ can be expected to be peaked in some directions, while not in other directions.

The peakedness of $\mathrm{P}[\check{\underline{a}}=z]$

We will measure peakedness of the PMF by means of the Ambiguity Dilution of Precision (ADOP). The ADOP was introduced in Teunissen (1997) and it is defined as ADOP = $\sqrt[2n]{|Q_{\hat{a}\hat{a}}|}$ (cycle). The ADOP is invariant for admissible ambiguity reparametrizations and it provides an easy-to-compute approximation to the ambiguity success-rate, i.e. probability of correct integer estimation $P[\underline{\check{a}}=a]\approx P_{\rm ADOP}=[2\Phi(\frac{1}{2{\rm ADOP}})-1]^n$. An ADOP smaller than 0.14 cycles corresponds with a $P_{\rm ADOP}$ larger than 0.99 (Odijk and Teunissen 2008).

We now first give a general expression of how the ADOP changes when extra parameters need to be estimated in the model.

Lemma 2 (ADOP under \mathcal{H}_0 and \mathcal{H}_a) The ADOP-change, when switching from \mathcal{H}_0 to \mathcal{H}_a , is given by

$$ADOP_{\mathcal{H}_a} = ADOP_{\mathcal{H}_0} \left(\frac{|Q_{\hat{c}\hat{c}}|}{|Q_{\hat{c}(a)\hat{c}(a)}|} \right)^{\frac{1}{2n}}$$
 (20)

This result shows that the change in ADOP and the change in precision of the bias-estimator act similarly as a law of communicating vessels. The more the bias-precision improves due to ambiguity fixing, the larger the ADOP gets. Hence, with the precision improvement of the bias estimator, one can expect the ambiguity success-rate to become poorer and possibly leading to the necessity of having to take more than one ambiguity probability mass into account.

To show how Lemma 2 works out for the GNSS model (13), we first take the determinant of the vc-matrix in the second equation of (15). As a result we get

$$|Q_{\hat{a}\hat{a}}| = |Q_{\hat{a}(c)\hat{a}(c)}||I_q + E^T Q_{\hat{a}(c)\hat{a}(c)}^{-1} E Q_{\hat{c}\hat{c}}|$$
(21)

with $E^TQ_{\hat{a}(c)\hat{a}(c)}^{-1}EQ_{\hat{c}\hat{c}}=[\frac{1}{\epsilon}\bar{C}_{\phi}^TQ^{-1}\bar{C}_{\phi}\ +\frac{1}{1+\epsilon}D^TQ^{-1}D]$ $[\bar{C}_p^TQ^{-1}\bar{C}_p]^{-1}$. Hence, the ADOP-ratio of the alternative hypothesis to the null-hypothesis follows as

$$\frac{\text{ADOP}_{\mathcal{H}_a}}{\text{ADOP}_{\mathcal{H}_0}} = \sqrt[2n]{|I_q + E^T Q_{\hat{a}(c)\hat{a}(c)}^{-1} E Q_{\hat{c}\hat{c}}|}$$
(22)

thus showing that the ratio can be expected to be large when $\operatorname{rank}(G, C_{\phi}) = p + q$ and small when $\operatorname{rank}(G, C_{\phi}) = p$. For q = 1 for example, we get the ADOP-ratio approximations

$$\frac{\text{ADOP}_{\mathcal{H}_a}}{\text{ADOP}_{\mathcal{H}_0}} \approx \begin{cases} \left(1 + \frac{1}{\epsilon} \frac{||\bar{C}_{\phi}||_Q^2}{|\bar{C}_p||_Q^2}\right)^{\frac{1}{2n}} & \text{if} \quad C_{\phi} \notin \mathcal{R}(G) \\ \left(1 + \frac{||D||_Q^2}{||\bar{C}_p||_Q^2}\right)^{\frac{1}{2n}} & \text{if} \quad C_{\phi} \in \mathcal{R}(G) \end{cases}$$

As we may assume the PMF of the integer estimated ambiguities under \mathcal{H}_0 to be very peaked, i.e. the \mathcal{H}_0 ambiguity success-rate to be very close to 1, the above shows that a similar peakedness can be expected of the PMF under \mathcal{H}_a in case $\mathrm{rank}(G, C_\phi) = p$, i.e. when the ADOP-ratio does not differ too much from 1. In case of $\mathrm{rank}(G, C_\phi) = p + q$ however, the ADOP-ratio is much larger due to the very small phase-code variance-ratio ϵ . As a consequence, the \mathcal{H}_a ambiguity success-rate can then be expected to differ significantly from 1, implying that nonnegligible probability masses can expected to be located at other integer ambiguity vectors than $a \in \mathbb{Z}^n$ as well.

On the integer-driven bias of $f_{\hat{c}(z)}(x)$

To measure the significance of the integer-driven bias $\Delta(z) = \mathrm{E}(\hat{\underline{c}}(z) - c)$, we consider its squared weighted norm with respect to the vc-matrix $Q_{\hat{c}(a)\hat{c}(a)}$,

$$\begin{split} ||\Delta z||_{Q_{\hat{c}(a)\hat{c}(a)}}^2 &= ||P_{\bar{C}}A(a-z)||_{Q_{yy}}^2 \\ &= ||\bar{C}^T Q_{yy}^{-1} \bar{A}(a-z)||_{Q_{\hat{c}(a)\hat{c}(a)}}^2 \\ &= ||(\bar{C}_{\phi} + \frac{\epsilon}{1+\epsilon} D)^T Q_{\phi\phi}^{-1} L(a-z)||_{Q_{\hat{c}(a)\hat{c}(a)}^{-1}\hat{c}(a)\hat{c}(a)}^2 \end{split}$$

from which it follows, together with (17) and (18), that

$$||\Delta z||_{Q_{\hat{c}(a)\hat{c}(a)}}^{2} \propto \begin{cases} \frac{1}{\sigma_{\phi}^{2}} & \text{if } C_{\phi} \notin \mathcal{R}(G) \\ \frac{1}{\sigma_{p}^{2}} & \text{if } C_{\phi} \in \mathcal{R}(G) \end{cases}$$
(23)

This shows, consistent with the peakedness of $f_{\hat{c}}(z)(x)$, that the integer-driven bias can expected to be significant when $C_{\phi} \notin \mathcal{R}(G)$ and less so otherwise. This measure of significance does however not give insight into where in c-space the integer-driven biases are projected to. To make this clearer, we symbolically write the infinite sum of the PDF $f_{\hat{c}}(x)$, cf. (11) under \mathcal{H}_0 , i.e. when c=0, as



$$PDF(\underline{\check{c}}|\mathcal{H}_{0}) = \\ \mathcal{N}_{q}(0,R)P[\underline{\check{a}} = a] + \\ \{\mathcal{N}_{q}(-c_{1},R) + \mathcal{N}_{q}(+c_{1},R)\}P[\underline{\check{a}} = z_{1}] + \\ \{\mathcal{N}_{q}(-c_{2},R) + \mathcal{N}_{q}(+c_{2},R)\}P[\underline{\check{a}} = z_{2}] + \cdots$$

$$(24)$$

in which $R=Q_{\hat{c}(a)\hat{c}(a)}, c_i=\bar{C}^+A(a-z_i)$, and where we made use of the symmetry of the PDF $f_{\underline{c}}(x)$ with respect to the origin, i.e. $P[\underline{\check{a}}=a+u]=P[\underline{\check{a}}=a-u]$ for all $u\in\mathbb{Z}^n$. If we assume the probability masses at z_i to be ordered as $P[\underline{\check{a}}=a]\geq P[\underline{\check{a}}=z_1]\geq P[\underline{\check{a}}=z_2]\geq ...$, then the largest peak of $f_{\underline{\check{c}}}(x)$ is centred at the origin, a second largest pair of peaks at $\pm c_1$, a third-largest pair of peaks at $\pm c_2$, etcetc. These locations and peak-sizes can be computed once the ordered ambiguity probability masses and their integer ambiguity vectors are known. This can be done efficiently with the LAMBDA 4.0 toolbox (Massarweh et al. 2025).

As an example of the above considerations, we use a single-epoch, double-differenced dual-frequency geometry-based GPS model and take the bias parameter c to be an ionospheric delay. In this case we have $C_{\phi} \notin \mathcal{R}(G)$, thus leading to a very peaked, phase-driven PDF $f_{\hat{c}(z)}(x)$. However, with the inclusion of the ionospheric delay, the ambiguity succes-rate drops from practically 1 to 0.61 under \mathcal{H}_a , thus giving a multimodal $f_{\underline{c}}(x)$, with 39% ambiguity probability mass contributing as scale factors to its noncentral modes. The result is shown in Fig. 3.

The AR significance test

In this section we introduce our ambiguity-resolved significance test and compare it with its AF- and AK counterparts.

Acceptance/rejection region

To be able to decide on the significance of an outcome of $\underline{\check{c}}$, we need a measure of significance, for which the *p*-value concept is often used. Assuming \mathcal{H}_0 to be correct, the

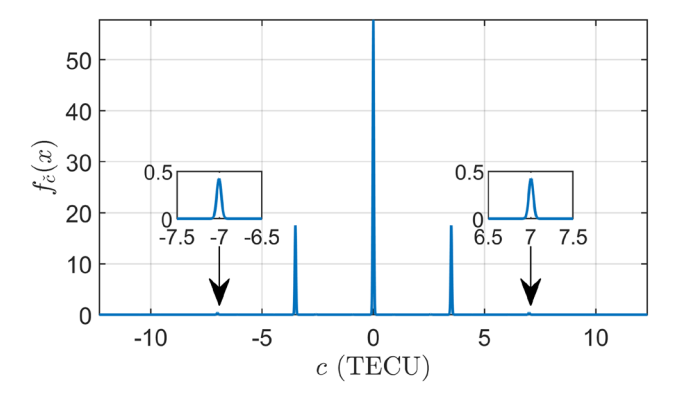
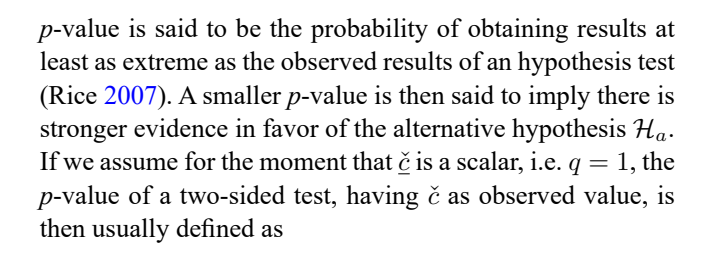


Fig. 3 Multimodal PDF of ambiguity-resolved ionospheric delay based on a single-epoch, dual-frequency, geometry-based GPS model, cf. skyplot Fig. 1



$$p = P[|\underline{\check{c}}| > |\check{c}| |\mathcal{H}_0] \tag{25}$$

thus implying that a value \check{c}_2 would be more extreme than \check{c}_1 if $P[\ |\check{\underline{c}}| > |\check{c}_1|\ |\mathcal{H}_0] > P[\ |\check{\underline{c}}| > |\check{c}_2|\ |\mathcal{H}_0]$. Although such conclusion may seem acceptable in case of unimodal distributions symmetric about zero, it appears odd for a multimodal distribution symmetric about zero. It would namely imply that \check{c}_2 -values close to off-centred modes could still be considered more extreme than \check{c}_1 -values residing elsewhere. Hence, for multimodal distributions, like the PDF of $\check{\underline{c}}$, an alternative approach is needed and one in which the modes of the distribution come into play as well. Here we therefore follow the *highest density* approach as also used in Teunissen (2007).

Let $\mathcal{A} \subset R^q$ be the acceptance region with false-alarm probability $P[\underline{\check{c}} \not\in \mathcal{A}|\mathcal{H}_0] = P[\underline{\check{c}} \in \mathcal{A}^c|\mathcal{H}_0] = \alpha$. Since we want the rejection to be rare when \mathcal{H}_0 is correct, the false alarm probability α is chosen as a small value. But since there are an infinite number of subsets that can produce this false alarm probability, we still need to determine a way of defining a proper \mathcal{A} . It seems reasonable to define the optimal subset as the one which has the acceptance probability $1-\alpha$ most concentrated, and thus captured in the smallest volume. Such subset is thus the solution to the minimization problem, $\min_{\mathcal{A} \subset R^q} V_{\mathcal{A}}$ subject to $P[\underline{\check{c}} \in \mathcal{A}|\mathcal{H}_0] = 1-\alpha$, where $V_{\mathcal{A}}$ denotes the volume of \mathcal{A} . The solution to this problem is given by the subset

$$\mathcal{A} = \{ x \in \mathbb{R}^q \mid f_{\check{c}}(x|\mathcal{H}_0) \ge \lambda_\alpha \} \tag{26}$$

where λ_{α} is chosen so as to satisfy the false-alarm constraint. For a proof, see Teunissen (2007), pp. 575–576. By a similar derivation one can also show that of all subsets with the same volume, \mathcal{A} captures the largest possible probability mass.

Subsets like (26) are referred to as highest density level sets and from their structure it follows that a more suitable p-measure than (25) would be

$$p = P[f_{\underline{\check{c}}}(\underline{\check{c}}) < f_{\underline{\check{c}}}(\check{c}) | \mathcal{H}_0]$$
(27)

Thus now \check{c}_2 would be considered more extreme than \check{c}_1 if the following inequality holds true: $P[f_{\underline{\check{c}}}(x|\mathcal{H}_0) < f_{\check{c}}(\check{c}_1|\mathcal{H}_0)] > P[f_{\check{c}}(x|\mathcal{H}_0) < f_{\check{c}}(\check{c}_2|\mathcal{H}_0)]$. Following this



GPS Solutions (2025) 29:200 Page 9 of 16 200

line of reasoning we define our ambiguity-resolved significance (ARs) test as follows.

Definition 1 (ARs-test) For sample \check{c} of \check{c} ,

Reject
$$\mathcal{H}_0$$
 if $f_{\check{c}}(\check{c}|\mathcal{H}_0) < \lambda_{\alpha}$ (28)

with λ_{α} chosen so as to satisfy a user-required false-alarm probability $P[\check{\underline{c}} \notin \mathcal{A} | \mathcal{H}_0] = \alpha$.

Two acceptance-region examples of the ARs-test are shown in Fig. 4. As the acceptance-region of the test is formed from subsets of highest density, the multimodality of a PDF may result in a disconnected acceptance region, as is shown in Fig. 4 (right). For a unimodal PDF, the acceptance-region is connected, as it would be when the traditional *p*-value concept, cf. (25) would be used. This is shown in Fig. 4(left).

ARs test sits in between AK and AF

We are now in a position to compare the ARs test with the AF- and AK-test, and show how they are limiting versions of the ARs test. In order to facilitate this comparison, we also write the AF- and AK-test, just like (28), in the form of a level-set of the PDF. We have:

Reject
$$\mathcal{H}_0$$
 if
$$\begin{cases} AF : f_{\underline{\hat{c}}}(\hat{c}|\mathcal{H}_0) < \mu_{\alpha} \\ ARs : f_{\underline{\hat{c}}}(\check{c}|\mathcal{H}_0) < \lambda_{\alpha} \\ AK : f_{\hat{c}(a)}(\hat{c}(a)|\mathcal{H}_0) < \nu_{\alpha} \end{cases}$$
(29)

with $\mu_{\alpha} = |2\pi Q_{\hat{c}\hat{c}}|^{-\frac{1}{2}} \exp\{-\frac{1}{2}\chi_{\alpha}^2(q,0)\}$ and $\nu_{\alpha} = |2\pi Q_{\hat{c}(a)\hat{c}(a)}|^{-\frac{1}{2}} \exp\{-\frac{1}{2}\chi_{\alpha}^2(q,0)\}$, and where \hat{c} , $\check{c} = \hat{c}(\check{a})$ and $\hat{c}(a)$ are the sample values of the respective statistics. Thus, in essence, if we want to compare the three tests, we can work with the three PDFs: $f_{\hat{c}}(x)$, $f_{\hat{c}(a)}(x)$, and $f_{\check{c}}(x)$.

First we compare $f_{\underline{\check{c}}}(x)$ with $f_{\underline{\hat{c}}(a)}(x)$. Since $f_{\underline{\check{c}}}(x) = \sum_{z \in \mathbb{Z}^n} f_{\underline{\hat{c}}(z)}(x) \mathrm{P}[\underline{\check{a}} = z]$, the multimodality of the PDF will get less with increasing ambiguity success-rate $\mathrm{P}[\check{a} = a]$ and in the limit give

Fig. 4 ARs-test acceptance region $\{x \in \mathbb{R}^q | f_{\underline{c}}(x|\mathcal{H}_0) \geq \lambda_\alpha \}$ of 5th (Left) and 6th (Right) PDF of Fig. 2 for $\alpha = 0.15$. As the 5th PDF is unimodal, its acceptance region is connected, while the multimodality of the 6th PDF, results in a disconnected acceptance region

$$\lambda_lpha$$
 $\int_{ ilde{\mathcal{E}}} (x|\mathcal{H}_0)$ 0 x

$$f_{ar{arrho}}(x|\mathcal{H}_0)$$

$$\lim_{P[\check{a}=a|\uparrow 1} f_{\underline{\check{c}}}(x) = f_{\underline{\hat{c}}(a)}(x) \tag{30}$$

Hence, in the limit, the ARs-test equals the AK-test and will then also have its excellent carrier-phase driven performance.

To compare $f_{\hat{c}}(x)$ with $f_{\check{c}}(x)$, we write

$$f_{\underline{\hat{c}}}(x) = \int f_{\underline{\hat{c}}\hat{a}}(x, v) dv$$

$$= \int f_{\underline{\hat{c}}|\underline{\hat{a}}}(x|v) f_{\underline{\hat{a}}}(v) dv$$

$$= \sum_{z \in \mathbb{Z}^n} \int_{S_z} f_{\underline{\hat{c}}|\underline{\hat{a}}}(x|v) f_{\underline{\hat{a}}}(v) dv$$
(31)

This shows, if $f_{\underline{\hat{c}}|\underline{\hat{a}}}(x|v)$ as function of v is flat over the pullin region S_z (this happens if the integer-grid is very dense with respect to the variability of the PDF, i.e. when the precision is poor), that $f_{\underline{\hat{c}}|\underline{\hat{a}}}(x|v) \approx f_{\underline{\hat{c}}(z)}(x)$ and therefore $f_{\underline{\hat{c}}}(x) \approx f_{\underline{\hat{c}}}(x)$. Hence, in this limit, the ARs-test equals the AF-test, with its usually much poorer performance.

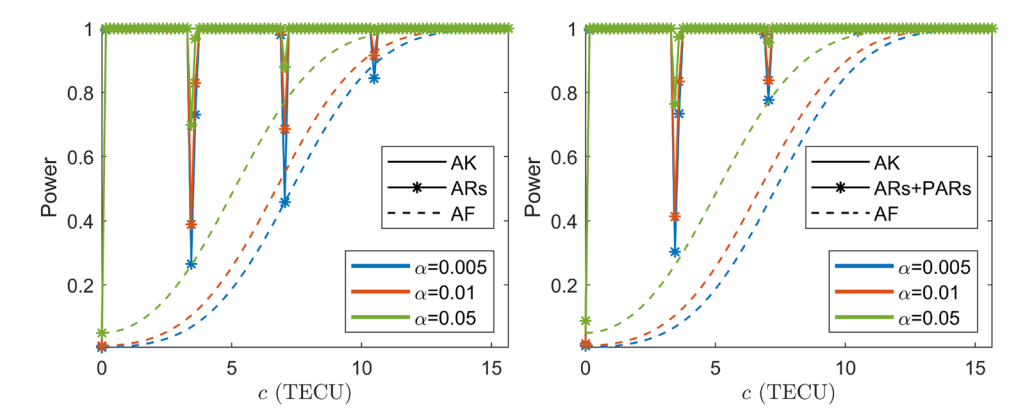
Just as the AK- and AF-tests, cf. (5), also the AR significance test (28) can shown to be a generalized likelihood ratio (GLR) test. With our null hypothesis being simple, $\mathcal{H}_0: c=0$, the GLR reads

$$GLR(x) = \frac{f_{\underline{c}}(x|c=0)}{\max_{c \in \mathbb{R}^q} f_{\underline{c}}(x|c)}$$
(32)

It then follows, with $x = \arg\max_{c \in \mathbb{R}^q} f_{\underline{\check{c}}}(x|c)$, noting $f_{\underline{\check{c}}}(x|x)$ is a constant, that $\operatorname{GLR}(\check{c}) < \lambda_\alpha/f_{\underline{\check{c}}}(\check{c}|\check{c})$ is equivalent to (28).

An example of the performance of the three significance tests is given in Fig. 5(Left). It shows the detection probabilities of the ionospheric significance tests as function of the bias c,

Fig. 5 Power functions of the AK, AF, ARs (Left) and ARs-combined (Right) ionospheric significance test for different false alarm probabilities α and based on a single-epoch, dual-frequency, geometry-based GPS model, cf. skyplot Fig. 1



$$P_{AF}(c) = P[f_{\underline{\hat{c}}}(\hat{c}) < \mu_{\alpha} | \mathcal{H}_{a}]$$

$$P_{ARs}(c) = P[f_{\underline{\hat{c}}}(\underline{\check{c}}) < \lambda_{\alpha} | \mathcal{H}_{a}]$$

$$P_{AK}(c) = P[f_{\hat{c}(a)}(\hat{c}(a)) < \nu_{\alpha} | \mathcal{H}_{a}]$$
(33)

The result shows, except for a few particular values of c, a superior performance of the ARs-test. The c-values for which the detection probability of the ARs-test drops in value, can be explained by the sharp multimodality of the PDF of $\underline{\check{c}}$, as shown in Fig. 3. These c values correspond with the mapped z-vectors for which the ambiguity probabilities $P[\check{\underline{a}}=z]$ are nonnegligible. For all other c-values, the power function is close to that of the AK-test and far superior to that of the AF-test.

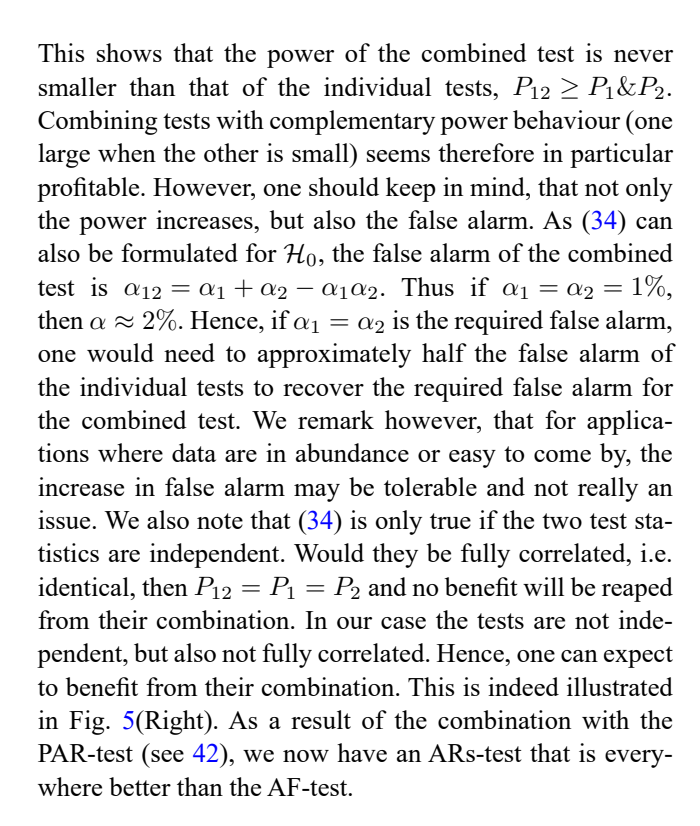
Combining tests

Despite the significant improvements the ARs-test brings, there is no guarantee that its power is everywhere better than that of the AF-test, as Fig. 5(Left) illustrates. Would one also like to improve on this situation, we introduce the idea of combining tests, in our case of the ARs-test with a partially ambiguity-resolved (PAR) version of it (see also Section "Partial ambiguity resolution based testing").

To describe the general idea of combining two tests for the same null-hypothesis, let the two tests be given as 'reject \mathcal{H}_0 if $T_1 > k_{\alpha_1}$ ' and 'reject \mathcal{H}_0 if $T_2 > k_{\alpha_2}$ '. Then it seems reasonable to have the combined test reject the null-hypothesis if one or both of the individual tests rejects the null-hypothesis, i.e. 'reject \mathcal{H}_0 if $T_1 > k_{\alpha_1}$ or $T_2 > k_{\alpha_2}$ '. To evaluate this combined test, one needs to determine its 'power' and 'false alarm'. This is not difficult to do if \underline{T}_1 and \underline{T}_2 are independent. Denoting the individual powers as $P_1 = P[\underline{T}_1 > k_{\alpha_1}|\mathcal{H}_a]$ and $P_2 = P[\underline{T}_1 > k_{\alpha_2}|\mathcal{H}_a]$, the power of the combined test becomes then

$$P_{12} = P[\{\underline{T}_1 > k_{\alpha_1}\} \cup \{\underline{T}_2 > k_{\alpha_2}\} | \mathcal{H}_a]$$

= $P_1 + P_2 - P_1 P_2$
= $1 - (1 - P_1)(1 - P_2)$ (34)



The AR normed significance test

As the ARs-test is based on the highest density region of the PDF $f_{\underline{c}}(x)$, its execution requires the evaluation of a weighted sum over the integers, cf. (11). Such is not needed if one would use the AK-test (10) as starting point and take the randomness of \underline{a} properly into account. In this section we therefore explore the characteristics of this AR normed (ARn) test and its relation to the ARs-test.



GPS Solutions (2025) 29:200 Page 11 of 16 200

The ARn-test

The ARn significance test is essentially the AK significance test, but then with a proper accounting of the uncertainty of the estimated integer ambiguities.

Definition 2 (*The ARn-test*) Let $\underline{\check{a}}$ be an admissible integer estimator of $a \in \mathbb{Z}^n$. Then the level- α ambiguity-resolved normed (ARn) test reads,

Reject
$$\mathcal{H}_0$$
 if $||\hat{c}(\check{a})||^2_{Q_{\hat{c}(a)\hat{c}(a)}} > k'_{\alpha}$ (35)

with critical value k'_{α} satisfying

$$P[||\underline{\hat{c}}(\underline{\check{a}})||_{Q_{\hat{c}(\alpha)\hat{c}(a)}}^2 > k_{\alpha}'|\mathcal{H}_0] = \alpha$$
(36)

Note that due to the inclusion of the uncertainty of $\underline{\check{a}}$, we have $k'_{\alpha} \neq k_{\alpha}$. We also remark that the test can be written in its PDF-form as

Reject
$$\mathcal{H}_0$$
 if $f_{\hat{c}(a)}(\check{c}) < \nu'_{\alpha}$ (37)

with $\nu_{\alpha}' = |2\pi Q_{\hat{c}(a)\hat{c}(a)}|^{-\frac{1}{2}} \exp\{-\frac{1}{2}k_{\alpha}'\}$, thus showing how it relates to the ARs-test, cf. Theorem 1 and (28). To execute the ARn-test we only need to compute the squared weighted norm of the sample $\check{c} = \hat{c}(\check{a})$. Also the PDF of ARn's test-statistic, $||\underline{\hat{c}}(\underline{\check{a}})||^2_{Q_{\hat{c}(a)\hat{c}(a)}}$, as well as the expression of its powerfunction, $P_{\text{ARn}}(c) = P[||\underline{\hat{c}}(\underline{\check{a}})||^2_{Q_{\hat{c}(a)\hat{c}(a)}} > k_{\alpha}'|\mathcal{H}_a]$, can be computed directly. We have the following result.

Theorem 3 (PDF and power of ARn-test) Let $\underline{\hat{a}}$ be the BLUE of a and $\underline{\check{a}}$ an admissible integer estimator of $E(\underline{\hat{a}}) = a \in \mathbb{Z}^n$. Then the PDF of $\underline{T} = ||\underline{\hat{c}}(\underline{\check{a}})||^2_{Q_{\hat{c}(a)\hat{c}(a)}}$ and the expression of the power function $P_{\mathrm{ARn}}(c) = P[\underline{T} > k'_{\alpha}|\mathcal{H}_a]$, are given as

$$f_{\underline{T}}(x|c) = \sum_{z \in \mathbb{Z}^n} f_{\underline{\chi}^2(q,\lambda_z)}(x) P[\check{a} = z]$$

$$P_{\text{ARn}}(c) = \sum_{z \in \mathbb{Z}^n} P[\underline{\chi}^2(q,\lambda_z) > k_{\alpha}'] P[\underline{\check{a}} = z]$$
(38)

with noncentrality parameter

$$\lambda_z = ||c + \bar{C}^+ A(a - z)||^2_{Q_{\hat{c}(a)\hat{c}(a)}}.$$

Proof see Appendix.

This result shows that the PDF of $\underline{T} = ||\hat{\underline{c}}(\underline{\check{a}})||^2_{Q_{\hat{c}(a)\hat{c}(a)}}$ is a weighted sum of noncentral Chi-square distributions with q degrees of freedom. Since the PDF of $||\underline{\check{c}}||^2_{Q_{\hat{c}(a)\hat{c}(a)}}$ is multimodal, it seems perhaps tempting to use, instead of the rejection region (35), the highest density as rejection region, just as it was done for $f_{\underline{\check{c}}}(x)$.

Such is however not a good choice, since this highest density rejection region will, in the limit when the ambiguity succes-rate goes to one, not become equal to that of the AK-test. Although the PDF goes in the limit to that of the AK test-statistic, $||\underline{\hat{c}}(a)||^2_{Q_{\hat{c}(a)\hat{c}(a)}}$, i.e.

$$\lim_{\mathbf{P}[\check{\underline{a}}=a]\uparrow 1} f_{||\hat{\underline{c}}(\check{\underline{a}})||^2_{Q_{\hat{c}(a)\hat{c}(a)}}}(x) = f_{||\hat{\underline{c}}(a)||^2_{Q_{\hat{c}(a)\hat{c}(a)}}}(x)$$

its highest density regions will generally *not* equal the rejection region of the AK-test, i.e. its performance will not be that of the AK-test.

ARn probability bounds

To characterize the error one makes when using the ARntest as if it is an AK-test, i.e. without taking the uncertainty of $\underline{\check{a}}$ into account, we now provide bounds on its false alarm and detection probabilities.

Corollary 1 (ARn probability bounds) Let $\underline{T} = ||\underline{\hat{c}}(\underline{\check{a}})||^2_{Q_{\hat{c}(a)\hat{c}(a)}}, \quad P[\underline{T} > k_{\alpha}|\mathcal{H}_{\theta}] = \alpha_n$ and $k_{\alpha} = \chi^2_{\alpha}(q,\theta)$ be the critical value of the level- α AK-test (5). Then

$$P[\underline{T} > k_{\alpha} | \mathcal{H}_a] \ge P_{AK}(c) P[\underline{\check{a}} = a]$$
 (39)

and

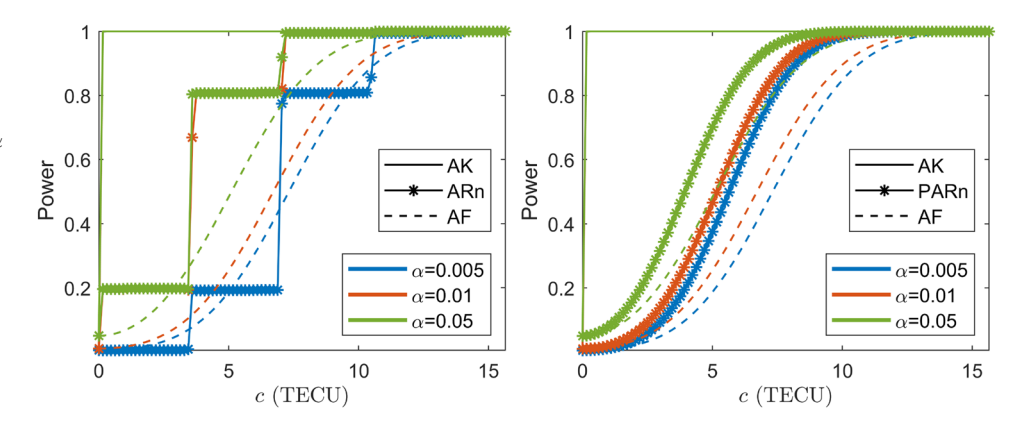
$$\alpha \le \alpha_n \le \alpha + (1 - \alpha)P[\underline{\check{a}} \ne a] \tag{40}$$

From the lower bound (39) we learn that for the same critical value k_{α} as used by the AK-test, the ARn detection probability is always larger than AK's power times the success-rate. This shows, as AK's power is usually very close to 1, that a high success-rate will also give a large detection probability $P[\underline{T} > k_{\alpha} | \mathcal{H}_a]$. Whether or not this translates in a similar high power for the ARn-test depends then on how much the critical value k_{α} differs from the level- α critical value k'_{α} of the ARn-test.

From the bounds of (40) we learn that, for the same critical value, ARn's probability of false alarm is never smaller than that of the AK-test and that the difference between these two probabilities becomes smaller, the larger the ambiguity success rate gets. Their difference can become quite large however in case the success-rate differs significantly from one. For the GNSS model used in Figs. 5 and 6, for instance, having a success-rate of $P[\underline{\tilde{u}}=a]=0.6137$, the actual ARn false alarm probabilities are $\alpha_n=0.3894$ when $\alpha=0.005$, $\alpha_n=0.3924$ when $\alpha=0.01$, and $\alpha_n=0.4170$ when $\alpha=0.05$. This shows the significant errors one will



Fig. 6 Power functions of ARn (Left) and PARn (Right) tests, compared with AF and AK ionospheric significance tests, for different false alarm probabilities α and based on a single-epoch, dual-frequency, geometry-based GPS model, cf. skyplot Fig. 1



make when applying the AK-test using samples from $\underline{\check{c}}$. Inequality (40) also implies that ARn's acceptance region will not be smaller than that of the AK-test, i.e. $k'_{\alpha} \geq k_{\alpha}$, and in fact it will often be much larger if their false alarm probabilities differ much.

As to the detection performance of the ARn-test, one should realize, although it converges to the exellent power performance of the AK-test when the success-rate goes to one, that the success-rate under \mathcal{H}_a may be significantly smaller than under \mathcal{H}_0 . Such case, having an ambiguity success-rate under \mathcal{H}_a of only 61%, is shown in Fig. 6(Left). It illustrates the performance of the ARn-test for the same GNSS model as considered in Figs. 3 and 5. The power functions shown are

$$P_{\text{AF}}(c) = P[f_{\underline{\hat{c}}}(\underline{\hat{c}}) < \mu_{\alpha} | \mathcal{H}_{a}]$$

$$P_{\text{ARn}}(c) = P[f_{\underline{\hat{c}}(a)}(\underline{\check{c}}) < \nu_{\alpha}' | \mathcal{H}_{a}]$$

$$P_{\text{AK}}(c) = P[f_{\hat{c}(a)}(\underline{\hat{c}}(a)) < \nu_{\alpha} | \mathcal{H}_{a}]$$
(41)

The staircase behaviour of ARn's powerfunction can be explained by the fact that the test uses a single connected acceptance region, while the multimodal PDF $f_{\underline{c}}(x)$ has very peaked conditional PDFs $f_{\underline{c}(z)}(x)$, cf. Figure 3. Hence, when $f_{\underline{c}}(x)$ translates over c under \mathcal{H}_a , its probability mass outside the acceptance region may remain constant for some time, before suddenly increasing again when another mode of the PDF exits the acceptance region. Although the ARntest has generally a larger power than the AF-test, especially for large α , there are also many instances in which it performs poorer than the AF-test.

Partial ambiguity resolution based testing

As the above explained performance of the ARn-test is due to the incompatibility of using a connected acceptance region for a multimodal PDF, improved performance may become feasible if multimodality can be avoided. Since multimodality of $f_{\hat{c}}(x)$ is due to the peakedness of $f_{\hat{c}(a)}$

and the flatness of $P[\underline{\tilde{a}}=z]$, the idea is to refrain from a full ambiguity resolution (FAR), but instead perform partial ambiguity resolution (PAR). One can then aim to have the PMF of the PAR-vector to be peaked, e.g. by having a required sufficiently high ambiguity success-rate of 0.999. Increasing the peakedness of the PMF, will of course go at the expence of the PDF-peakedness of the partially ambiguity constrained bias vector. It is therefore their combined effect that determines whether or not improved performance can be achieved.

The PAR-method that we apply is the one originally introduced in Teunissen et al. (1999), see also Massarweh et al. (2025). The FAR and PAR versions of the ARn-test are then

Reject
$$\mathcal{H}_0$$
 if $\left\{ \begin{array}{l} \mathrm{FAR} : f_{\hat{\mathcal{C}}(a)}(\check{c}) < \nu'_{\alpha} \\ \mathrm{PAR} : f_{\hat{\mathcal{C}}(a_1)}(\check{c}_1) < \nu''_{\alpha} \end{array} \right.$ (42)

with

$$\underline{\check{c}} = \underline{\hat{c}} - Q_{\hat{c}\hat{a}} Q_{\hat{a}\hat{a}}^{-1} (\underline{\hat{a}} - \underline{\check{a}})$$

$$\underline{\check{c}}_1 = \underline{\hat{c}} - Q_{\hat{c}\hat{a}_1} Q_{\hat{a}_1\hat{a}_1}^{-1} (\underline{\hat{a}}_1 - \underline{\check{a}}_1)$$
(43)

in which a_1 is the vector of subset ambiguities as selected by the PAR-method. The PAR-version of the ARn-test will be referred to as the PARn-test. The required PAR successrate is set at 99.9%.

Figure 6(Right) shows, for the same model as used in Fig. 6(Left), how the power function of the PARn-test, $P_{\mathrm{PARn}}(c) = \mathrm{P}[f_{\hat{\mathcal{E}}(a_1)}(\check{\mathcal{E}}_1) < \nu_{\alpha}''|\mathcal{H}_a]$, compares with those of the AF- and AK-test. The result shows that now, due to partial ambiguity resolution, the relatively simple to execute PARn-test achieves a performance that is superior to that of the AF-test for all c.



GPS Solutions (2025) 29:200 Page 13 of 16 200

Summary and conclusions

In this contribution we introduced a parameter significance test for carrier-phase GNSS. Our test differs from existing significance tests in that it takes the unknown integerness of the ambiguities rigorously into account when testing the hypotheses of (2). The test is constructed from PDF level sets of the mixed-integer estimator $\underline{\check{c}}$ of the unknown biasestimator $c \in \mathbb{R}^q$. The test sits in between the ambiguity-known (AK) significance test and the ambiguity-float (AF) significance test, in the sense that it converges to the AK-test in case the ambiguity success-rate goes to one, $P[\underline{\check{a}}=a]\uparrow 1$, while converging to the performance of the AF-test the more dense the integer grid becomes.

The quality of the test is driven by the PDF of $\underline{\check{c}}$,

$$f_{\underline{\check{c}}}(x) = \sum_{z \in \mathbb{Z}^n} f_{\underline{\hat{c}}(z)}(x) P[\underline{\check{a}} = z]$$
(44)

which on its turn is driven by the PDF of the conditional bias-estimator $\hat{c}(z)$ and the PMF of the integer ambiguity estimator \check{a} . The PDF is symmetric with respect to c, at which point it also reaches its maximum. Its shape is determined by the peakedness of $P[\underline{\check{a}} = z]$ and the locations and peakedness of $f_{\hat{c}(z)}(x)$, cf. Figure 2. Ideally one would like $f_{\hat{c}(z)}(x)$ peaked and $P[\underline{\check{a}}=a]\approx 1$. It was shown however that such ideal case is difficult to realize in general. For the ambiguity success-rate under \mathcal{H}_a to be as large as under \mathcal{H}_0 , the float-estimators \hat{c} and \hat{a} need to be uncorrelated, thus implying that then no benefits for the bias-estimator can be reaped from ambiguity resolution, i.e. $\hat{c}(a) = \hat{c}$. We have also shown, with reference to the 'law of communicating vessels', that the more the bias-estimator profits from ambiguity-constraining, the less likely it is that the precision of the ambiguities can stay at the level of \mathcal{H}_0 , cf. Lemma 2. It is therefore the actual interplay between $f_{\hat{c}(z)}(x)$ and $P[\underline{\check{a}} = z]$ in (44) that will ultimately determine the performance of the test.

To infer the situation for GNSS, we considered the challenging single-epoch GNSS model, which was assumed full rank, both under \mathcal{H}_0 and \mathcal{H}_a . It was shown, if $[G,C_\phi]$ has maximum rank p+q, that the PDF $f_{\underline{\tilde{c}}(z)}(x)$ is phase-driven and the PMF $P[\underline{\tilde{a}}=z]$ code-driven. In this case one can expect the PDF $f_{\underline{\tilde{c}}}(x)$ to be multimodal with several sharp modes, the number of which depends on the number of nonneglible probability masses $P[\underline{\tilde{a}}=z]$. The ionospheric delay case was given as one such example, cf. Figure 3. When $[G,C_\phi]$ has minimum rank p, then both $f_{\underline{\hat{c}}(z)}(x)$ and $P[\underline{\check{a}}=z]$ will be code-driven. In such case, the PDF $f_{\underline{\tilde{c}}}(x)$ may become unimodal, an example being when one tests for code outliers.

In formulating our significance test, we discussed the necessity of abandoning the classical 'p-value' approach as it fails to do justice to the multimodality of $f_{\underline{\xi}}(x)$. Instead a level-set approach was used (Teunissen 2007), thus allowing to capture the PDF's highest density regions for acceptance of the null-hypothesis, cf. Figure 4. Hence, its power function is given as

$$P_{\text{ARs}}(c) = P[f_{\check{c}}(\underline{\check{c}}|\mathcal{H}_a) < \lambda_{\alpha}] \tag{45}$$

with false alarm probability $\alpha = P[f_{\underline{\check{c}}}(\underline{\check{c}}|\mathcal{H}_0) < \lambda_{\alpha}]$. It was shown under which circumstances the test outperforms the AF-test, thereby then often even providing a power close to that of the AK-test, cf. Figure 5.

We also introduced, with a dual purpose, the ambiguityresolved normed (ARn) test. First we used it to illustrate the poor false alarm performance of the AK-test when applied with samples of č, cf. Corollary 1. When neglecting the uncertainty of \check{a} , as one does with the AK-test, the actual false alarms were shown to be very much larger than that assumed by the AK-test. Secondly, we showed the ARn-test to be an easier-to-compute approximation of the ARs-test, cf. (37). How well this approximation works depends on the modality of $f_{\check{c}}(x)$. As the approximation is excellent in the unimodal case, the concept of PAR-based testing was introduced. By means of partial ambiguity resolution, multimodality in the PDF of the ambiguity-resolved bias-estimator is avoided and a test is obtained with an everywhere better power than the AF-test, cf. Figure 6. It was thereby also shown how partial and full ambiguity-resolved significance testing can be combined to further improve testing performance.

Appendix

Proof of Lemma 1 (Bias precision and noncentrality): The reduced system of normal equations of the model $E(\underline{y}) = Aa + Bb + Cc$, $D(\underline{y}) = Q_{yy}$ is $\bar{C}^T Q_{yy}^{-1} \ \bar{C} \underline{\hat{c}} = \bar{C}^T \ Q_{yy}^{-1} \underline{y}$, with $\bar{C} = P_{[A,B]}^{\perp} C$, from which the result $Q_{\hat{c}\hat{c}} = (\bar{C}^T Q_{yy}^{-1} \bar{C})^{-1}$ follows. Similarly, the reduced system of normal equations of the model $E(\underline{y} - Aa) = Bb + Cc$, $D(\underline{y}) = Q_{yy}$ is $\bar{C}^T Q_{yy}^{-1} \bar{C} \underline{\hat{c}} (a) = \bar{C}^T Q_{yy}^{-1} (\underline{y} - Aa)$, with $\bar{C} = P_B^{\perp} C$, from which the result $Q_{\hat{c}(a)\hat{c}(a)} = (\bar{C}^T Q_{yy}^{-1} \bar{C})^{-1}$ follows. For the noncentrality parameter we have, with $\bar{A} = P_B^{\perp} A$ and $P_{[A,B]} = P_{\bar{A}} + P_B$,



$$\lambda_{\hat{c}} = c^T Q_{\hat{c}\hat{c}}^{-1} c$$

$$= c^T \bar{C}^T Q_{yy}^{-1} \bar{C} c$$

$$= c^T C^T Q_{yy}^{-1} P_{[A,B]}^{\perp} C c$$

$$= c^T C^T Q_{yy}^{-1} [P_{\bar{A}}^{\perp} - P_{\bar{A}}] C c$$

$$= \lambda_{\hat{c}(a)} - ||P_{\bar{A}} C c||_{Q_{yy}}^2$$
(46)

from which the result follows.

Proof of Theorem 1 (PDF AR-bias estimator): The float ambiguity solution of model $E(\underline{y}) = Aa + Bb + Cc$, $D(\underline{y}) = Q_{yy}$ follows from solving the reduced system of normal equations $\bar{A}^TQ_{yy}^{-1}\bar{A}\hat{\underline{a}} = \bar{A}^TQ_{yy}^{-1}\underline{y}$, where $\bar{A} = P_{[B,C]}^{\perp}A$. It is distributed as $\hat{\underline{a}} \sim \mathcal{N}_n(a,Q_{\hat{a}\hat{a}}=(\bar{A}^TQ_{yy}^{-1}\bar{A})^{-1})$. For any admissible integer estimator $\underline{\check{a}} = \mathcal{I}(\hat{\underline{a}}), \ \mathcal{I}: \mathbb{R}^n \mapsto \mathbb{Z}^n$, with pull-in regions $S_z = \{x \in \mathbb{R}^n | z = \mathcal{I}(x)\}$, the PMF is given as $P[\underline{\check{a}} = z] = \int_{S_z} f_{\underline{\hat{a}}}(x)dx$. The z-constrained bias solution $\hat{\underline{c}}(z)$ follows from solving the reduced normal equations $\bar{C}^TQ_{yy}^{-1}\bar{C}\hat{\underline{c}}(z) = \bar{C}^TQ_{yy}^{-1}(\underline{y} - Az)$. It is distributed as $\hat{\underline{c}}(z) \sim \mathcal{N}_q(c + \bar{C}^TQ_{yy}^{-1}A(a - z), Q_{\hat{c}(a)\hat{c}(a)})$, whereby we note that $\hat{\underline{a}}$ and $\hat{\underline{c}}(z)$ are independent. We therefore may write for $\underline{\check{c}} = \hat{\underline{c}}(\underline{\check{a}})$,

$$\begin{split} \mathbf{P}[\underline{\check{c}} \in \Omega] &= \sum_{z \in \mathbb{Z}^n} \mathbf{P}[\underline{\hat{c}}(\underline{\check{a}}) \in \Omega | \underline{\check{a}} = z] \mathbf{P}[\underline{\check{a}} = z] \\ &= \sum_{z \in \mathbb{Z}^n} \mathbf{P}[\underline{\hat{c}}(z) \in \Omega | \underline{\check{a}} = z] \mathbf{P}[\underline{\check{a}} = z] \\ &= \sum_{z \in \mathbb{Z}^n} \mathbf{P}[\underline{\hat{c}}(z) \in \Omega] \mathbf{P}[\underline{\check{a}} = z] \end{split}$$

As this result holds true for any $\Omega \subset \mathbb{R}^n$, the result follows.

Proof of Theorem 2 (GNSS PDF $f_{\underline{\check{c}}}(x)$ characterized): For model $\mathrm{E}(\underline{y}) = Aa + Bb + Cc$, $\mathrm{D}(\underline{y}) = Q_{yy}$, the b-reduced normal matrix, or inverse vc-matrix of $(\hat{\underline{a}}^T, \hat{\underline{c}}^T)^T$, is given as

$$\begin{bmatrix} N_{\hat{a}\hat{a}} & N_{\hat{a}\hat{c}} \\ N_{\hat{c}\hat{a}} & N_{\hat{c}\hat{c}} \end{bmatrix} = \begin{bmatrix} \bar{A}^T Q_{yy}^{-1} \bar{A} & \bar{A}^T Q_{yy}^{-1} \bar{C} \\ \bar{C}^T Q_{yy}^{-1} \bar{A} & \bar{C}^T Q_{yy}^{-1} \bar{C} \end{bmatrix}$$
(47)

with $\bar{A}=P_B^\perp A$ and $\bar{C}=P_B^\perp C$. When applied to the single-epoch GNSS model (13), using $Q_{yy}=\sigma_p^2$ \times blockdiag $(Q,\epsilon Q)$, we find for \bar{A} and \bar{C} ,

$$\bar{A} = \begin{bmatrix} -\frac{1}{1+\epsilon} P_G \\ P_G^{\perp} + \frac{\epsilon}{1+\epsilon} P_G \end{bmatrix} L \tag{48}$$

and

$$\bar{C} = \begin{bmatrix} P_G^{\perp} C_p + \frac{1}{1+\epsilon} P_G(C_p - C_{\phi}) \\ P_G^{\perp} C_{\phi} - \frac{\epsilon}{1+\epsilon} P_G(C_p - C_{\phi}) \end{bmatrix}$$

$$(49)$$

First we prove the results pertaining to the conditional PDF $f_{\hat{c}(z)}(x)$, i.e. the results of (14). As $Q_{\hat{c}\hat{c}}=[N_{\hat{c}\hat{c}}-N_{\hat{c}\hat{a}}N_{\hat{a}\hat{c}}^{-1}N_{\hat{a}\hat{c}}]^{-1}$, it follows from (47), (48) and (49), recognizing that L is invertible, that $Q_{\hat{c}\hat{c}}=[\bar{C}_p^TQ_{pp}^{-1}\bar{C}_p]^{-1}$, which proves the first equation of (14). Similarly, substitution of (49) into $Q_{\hat{c}(a)\hat{c}(a)}=N_{\hat{c}\hat{c}}^{-1}=(\bar{C}Q_{yy}^{-1}\bar{C})^{-1}$, proves the second equation of (14). For the integer-driven shifts, $\Delta(z)=\mathrm{E}(\hat{c}(z)-c)$, we may write

$$\Delta(z) = -Q_{\hat{c}\hat{a}}Q_{\hat{a}\hat{a}}^{-1}(a-z)$$

$$= +N_{\hat{c}\hat{c}}^{-1}N_{\hat{c}\hat{a}}(a-z)$$

$$= +Q_{\hat{c}(a)\hat{c}(a)}\bar{C}^{T}Q_{yy}^{-1}\bar{A}(a-z)$$
(50)

which, upon substitution of (48) and (49), proves the third equation of (14).

We now prove (15). Its first equation follows from substituting (48) into $Q_{\hat{a}(c)\hat{a}(c)}=N_{\hat{a}\hat{a}}^{-1}=(\bar{A}^TQ_{yy}^{-1}\bar{A})^{-1}$, thereby recognizing that L is invertible. To prove the second equation, we first write

$$Q_{\hat{a}\hat{a}} = Q_{\hat{a}(c)\hat{a}(c)} + N_{\hat{a}\hat{a}}^{-1} N_{\hat{a}\hat{c}} Q_{\hat{c}\hat{c}} N_{\hat{c}\hat{a}} N_{\hat{a}\hat{a}}^{-1}$$
(51)

which follows from $Q_{\hat{a}(c)\hat{a}(c)} = Q_{\hat{a}\hat{a}} - Q_{\hat{a}\hat{c}}Q_{\hat{c}\hat{c}}^{-1}Q_{\hat{c}\hat{a}}$ and $Q_{\hat{a}\hat{c}}Q_{\hat{c}\hat{c}}^{-1} = -N_{\hat{a}\hat{a}}^{-1}N_{\hat{a}\hat{c}}$. Substitution of (48) and (49) into $N_{\hat{a}\hat{a}}^{-1}N_{\hat{a}\hat{c}} = (\bar{A}^TQ_{yy}^{-1}\bar{A})^{-1}\bar{A}^TQ_{yy}^{-1}\bar{C}$ proves the second equation of (15).

Proof of Lemma 2 (ADOP under \mathcal{H}_0 and \mathcal{H}_a): The determinant of a partitioned positive definite matrix can be factored in a product of determinants as

$$\begin{vmatrix} \begin{bmatrix} Q_{\hat{a}\hat{a}} & Q_{\hat{a}\hat{c}} \\ Q_{\hat{c}\hat{a}} & Q_{\hat{c}\hat{c}} \end{bmatrix} \end{vmatrix} = |Q_{\hat{a}\hat{a}}||Q_{\hat{c}(a)\hat{c}(a)}|$$

$$= |Q_{\hat{c}\hat{c}}||Q_{\hat{a}(c)\hat{a}(c)}|$$
(52)

with the conditional vc-matrices $Q_{\hat{c}(a)\hat{c}(a)} = Q_{\hat{c}\hat{c}}$ $-Q_{\hat{c}\hat{a}}Q_{\hat{a}\hat{c}}^{-1}Q_{\hat{c}\hat{c}}$ and $Q_{\hat{a}(c)\hat{a}(c)} = Q_{\hat{a}\hat{a}} - Q_{\hat{a}\hat{c}}Q_{\hat{c}\hat{c}}^{-1}Q_{\hat{c}\hat{a}}$.



GPS Solutions (2025) 29:200 Page 15 of 16 200

Proof of Theorem 3 (PDF and power of ARn-test): As $||\underline{\hat{c}}(z)||^2_{Q_{\hat{c}(a)\hat{c}(a)}} \sim \chi^2(q,\lambda_z)$ and $\underline{\hat{c}}(z)$ and $\underline{\hat{a}}$ are independent, we have for any interval $\Omega \subset \mathbb{R}^+_0$,

$$\begin{split} \mathbf{P}[\underline{T} \in \Omega] &= \mathbf{P}[||\hat{\underline{c}}(\underline{\check{a}})||^2_{Q_{\hat{c}(a)\hat{c}(a)}} \in \Omega] \\ &= \sum_{z \in \mathbb{Z}^n} \mathbf{P}[||\hat{\underline{c}}(z)||^2_{Q_{\hat{c}(a)\hat{c}(a)}} \in \Omega, \underline{\check{a}} = z] \\ &= \sum_{z \in \mathbb{Z}^n} \mathbf{P}[||\hat{\underline{c}}(z)||^2_{Q_{\hat{c}(a)\hat{c}(a)}} \in \Omega] \mathbf{P}[\underline{\check{a}} = z] \\ &= \sum_{z \in \mathbb{Z}^n} \mathbf{P}[\underline{\chi}^2(q, \lambda_z) \in \Omega] \mathbf{P}[\underline{\check{a}} = z] \end{split}$$

from which (38) follows. Substitution of (38) into $P_{\rm ARn}(c)$ = $P[\underline{T} > k_{\alpha}'|c] = \int_{k_{\alpha}'}^{\infty} f_{\underline{T}}(x|c)dx$ gives the sought for expression of the power function.

Proof of Corollary 1 (ARn probability bounds): We first prove (39). From (38) follows

$$P[\underline{T} \in \Omega] = \sum_{z \in \mathbb{Z}^n} P[\underline{\chi}^2(q, \lambda_z) \in \Omega] P[\underline{\check{a}} = z]$$
(53)

Since all terms in the infinite sum are non-negative, we have

$$P[\underline{T} \in \Omega] \ge P[\chi^2(q, 0) \in \Omega] P[\underline{\check{a}} = a]$$
(54)

From this inequality follows (39) by setting $\Omega=(k_{\alpha},\infty)$. By setting $\Omega=[0,k_{\alpha}]$ and c=0, it also follows from (54) that $1-\alpha_n\geq (1-\alpha)\mathrm{P}[\underline{\check{a}}=a]$, which gives the upper bound of (40). To determine the lower bound, we use $\mathrm{P}[\underline{\chi}^2(q,0)>k_{\alpha}]\leq \mathrm{P}[\underline{\chi}^2(q,\lambda)>k_{\alpha}]$, from which it follows for c=0 from (53) that $\mathrm{P}[\underline{T}>k_{\alpha}]\geq \mathrm{P}[\underline{\chi}^2(q,0)>k_{\alpha}]=\alpha$.

Acknowledgements The numerical and graphical results were created and provided by Chengyu Yin, and both he and Christian Tiberius provided feedback and corrections to earlier versions of this contribution.

Author Contributions This is a single-author paper

Data Availability No datasets were generated or analysed during the current study.

Declarations

Conflict of interest The authors declare no conflict of interest.

Open Access This article is licensed under a Creative Commons Attribution 4.0 International License, which permits use, sharing, adaptation, distribution and reproduction in any medium or format, as long as you give appropriate credit to the original author(s) and the source, provide a link to the Creative Commons licence, and indicate if changes were made. The images or other third party material in this article are included in the article's Creative Commons licence, unless

indicated otherwise in a credit line to the material. If material is not included in the article's Creative Commons licence and your intended use is not permitted by statutory regulation or exceeds the permitted use, you will need to obtain permission directly from the copyright holder. To view a copy of this licence, visit http://creativecommons.org/licenses/by/4.0/.

References

- Biagi L, Grec FC, Negretti M (2016) Low-cost GNSS receivers for local monitoring: experimental simulation, and analysis of displacements. Sensors 16:2140. https://doi.org/10.3390/s16122140
- Huang G, Du S, Wang D (2023) GNSS techniques for real-time monitoring of landslides: a review. Satell Navig 4(5):10
- Hofmann-Wellenhof B, Lichtenegger H, Wasle E (eds.) (2008) GNSS: global navigation satellite systems. In: GPS, GLONASS, Galileo and More. Springer, New York
- Khanafseh S, Pullen S, Warburton J (2012) Carrier phase ionospheric gradient ground monitor for GBAS with experimental validation. J Inst Navig 59:51–60
- Leick A, Rapoport L, Tatarnikov D (2015) GPS satellite surveying, 4th edn. Wiley, Hoboken
- Morton Y, Diggelen F, Spilker J Jr, Parkinson B, Lo S, Gao G (eds) (2020) Position, navigation, and timing technologies in the 21st century: integrated satellite navigation, sensor systems, and civil applications. Wiley, Hoboken
- Massarweh L, Verhagen S, Teunissen PJG (2025) New LAMBDA toolbox for mixed-integer models: estimation and evaluation. GPS Solut 29:14
- Odijk D, Teunissen PJG (2008) ADOP in closed form for a hierarchy of multi-frequency single-baseline GNSS models. J Geod 82:473–492
- Perfetti N (2006) Detection of station coordinate discontinuities within the Italian GPS fiducial network. J Geod 80(7):381–396
- Rice JA (2007) Mathematical statistics and data analysis, 3rd edn. Duxbury Advanced Series
- Strang G, Borre K (1997) Linear algebra, geodesy and GPS. Welleslev-Cambridge Press, Welleslev
- Teunissen PJG, Bakker PF (2013) Single-receiver single-channel multi-frequency GNSS integrity: outliers, slips, and ionospheric disturbances. J Geod 87:161–177
- Teunissen PJG (1997) A canonical theory for short GPS baselines. Part I: The baseline precision, Part II: The ambiguity precision and correlation, Part III: The geometry of the ambiguity search space, Part IV: Precision versus reliability. J Geod 71(6):320-336, 71(7): 389-401, 71(8): 486-501, 71(9): 513-525
- Teunissen PJG (1998) Success probability of integer GPS ambiguity rounding and bootstrapping. J Geod 72:606–612
- Teunissen PJG (1999) An optimality property of the integer least-squares estimator. J Geod 73:587–593
- Teunissen PJG (2003) Theory of integer equivariant estimation with application to GNSS. J Geod 77:402–410. https://doi.org/10.1007/s00190-003-0344-3
- Teunissen PJG (2007) Least-squares prediction in linear models with integer unknowns. J Geod 81:565–579
- Teunissen PJG (2010) Mixed integer estimation and validation for next generation GNSS. In: Freeden W et al. (eds) Chapter 37 in handbook of geomathematics, pp 1102–1127
- Teunissen PJG (2024) The ambiguity-resolved detector: a detector for the mixed-integer GNSS model. J Geod 98:83
- Teunissen PJG, Joosten P, Tiberius CCJM (1999) Geometry-free ambiguity success rates in case of partial fixing. In: Proceedings of ION ITM, San Diego, CA, USA, pp 201–207



200 Page 16 of 16 GPS Solutions (2025) 29:200

Teunissen PJG, Montenbruck O (eds) (2017) Springer handbook of global navigation satellite systems. Springer, Cham

- Teunissen PJG, Massarweh L, Verhagen S (2021) Vectorial integer bootstrapping: flexible integer estimation with application to GNSS. J Geod 95:99
- Yin C, Teunisse PJG, Tiberius CCJM (2024) Implementation of ambiguity-resolved detector for high-precision GNSS fault detection. In: Proceedings ION GNSS+ 2024, Baltimore, Maryland, pp 2163–2174
- Yin C, Teunissen PJG, Tiberius CCJM (2025) Performance of ambiguity-resolved detector for GNSS mixed-integer model. GPS Solut 29:76
- Yu Y, Yang L, Shen Y, Sun N (2023) A DIA method based on maximum a posteriori estimate for multiple outliers. GPS Solut 27:199
- Zeng J, Zhang Z, He X, Yuan Y, Li Y, Song M (2023) Real-time GNSS multiple cycle slip detection and repair based on a controllable geometry-based method in relative positioning. Measurement 216:112940

Publisher's Note Springer Nature remains neutral with regard to jurisdictional claims in published maps and institutional affiliations.

